Dynamical Systems Approach to Fatigue Damage Identification

David Chelidze[*] **and** **Ming Liu**

Department of Mechanical Engineering & Applied Mechanics

University of Rhode Island

Abstract

In this paper, we present a dynamical systems approach to material damage identification. This methodology does not depend on knowledge of the particular damage physics of material fatigue. Instead, it provides experimental means to determine what are practically observable and observed facts of damage accumulation, thus making it possible to develop or experimentally verify appropriate damage evolution laws. A concept of phase space warping is used to develop new damage tracking feature vectors from measured time series through phase space reconstruction. These feature vectors provide critical information about the dimensionality of a damage process that was missing from an old scalar metric described in previous work. Damage identification is achieved by applying either proper orthogonal decomposition (POD) or smooth orthogonal decomposition (SOD) to these vectors. The method is experimentally validated using an elasto-magnetic system, in which a harmonically forced cantilever beam in a nonlinear magnetic field accumulates fatigue damage. Both damage identification methods yield a single active damage mode that shows power-law type monotonic trends, which is also consistent with a result obtained using the old scalar metric. These results are shown to be in good agreement with the Paris fatigue crack growth model during the time-period of macroscopic crack growth. Using this simple model, accurate time to failure predictions are shown well ahead of actual beam fracture. In addition, this identification scheme provides much needed insight into the dimensionality of incipient or early fatigue damage accumulation process, which is shown to be describable by only one scalar damage variable for this specific experiment.

[*]corr. author ⋄ email: chelidze@egr.uri.edu ⋄ phone: 401.874.2356 ⋄ fax: 401.874.2355 ⋄ http://www.mce.uri.edu/chelidze

1

1 Introduction

Scientific and engineering literature abounds with material damage models based on physical insights or empirical observation. These models are usually focused on mechanics of fatigue damage accumulation [1–5]. Despite the variety of approaches to model the mechanics of fatigue, there is a clear lack of practical methods for tracking *incipient* fatigue damage in operating machinery. There are several reasons for this discrepancy. First, although physics-based damage models are relatively easy to verify in simple experimental systems using beams or plates subjected to constant amplitude cyclic loading, they are usually unable to provide valid models of fatigue damage accumulation in complex forcing environments. Furthermore, most of these models ignore basic observability of their damage states (i.e., crack length) in practical, real-life situations (e.g., when the direct measurement of a crack size is impossible or impractical). Secondly, almost all statistical (cycle counting) damage models gloss over the role that the initial damage state has on the true life cycle of structures [6].

The dynamical systems approach to damage evolution [7] brings new insights to traditional damage physics. It provides a consistent, robust and abstract mathematical framework for exploring damage evolution dynamics. In addition, it enables one to relate experimental measurements to theoretical or empirical damage evolution laws. Damage in machinery or structural systems is a complex phenomenon that can manifest itself in many different modes. In this paper, we make no attempt to theorize about the "hidden" physical nature of damage. Instead, we aim to develop appropriate concepts and procedures for identifying phenomenological (empirical) regularities from analysis of measured time series. These developments do not rely on a physical description of damage, but we demonstrate that they are consistent with such physics-based models.

The approach proposed here is to determine experimentally the observable and observed facts about particular damage in a simple experiment with the aim of formulating phenomenological regularities. Consequently, experimental links can be established between the data-based metrics and complex, "hidden" damage phenomena. As a result, one acquires the ability to develop practical empirical (phenomenological) damage evolution laws and to experimentally validate available first-principles damage models. Damage laws that are developed or validated in this way will have the proper physical characteristics and appropriate time and spatial scales for practical damage diagnosis and prognosis applications.

In the next section, a brief overview of related literature is used to frame our approach to damage diagnosis. A brief description of our previously presented damage tracking procedure is given in the following section, with new improvements and additions. We also demonstrate the application of the described techniques to an experimental magneto-elastic system with accumulating fatigue damage. Finally, the results of experimental damage identification, failure prediction and their implications are discussed, followed by conclusions.

2 Background

Fatigue damage accumulation spans multiple length scales of micro- and macromechanics of fracture. Solid-state physics and material science study the subject of dislocations and submicrocracks. These phenomena describe the damage initiation in materials characterized by $10^{-9} \ldots 10^{-7}$ m length scales. However, the solid-state theories describing the physics at these length scales are not appropriate for prediction of material properties due to the large number of discrete damage levels. In *continuum damage mechanics* (CDM) [4, 8, 9], the state space of incipient damage is very high dimensional, but nonetheless the explicit evolution equations are available. This theory deals with the subject of micro- and small macrocracks that are distributed in the material characterized by $10^{-6} \ldots 10^{-2}$ m length scales. Finally, large macroscopic cracks are the subject of mechanics of solids and structures, i.e. macromechanics of fracture. In *fracture mechanics* [10–13] the damage state space is quite low dimensional, however, these evolution equations as well as CDM are difficult to relate to online measurements.

In *machinery and structural health monitoring* (MSHM) systems, we are faced with the problem of relating numerous system measurements back to the appropriate damage state. Therefore, the important and natural questions that need to be answered are (a) what are the appropriate damage states that can be tracked with available measurements? (b) how can this tracking be accomplished? and (c) what is the appropriate damage evolution law that can be used for predicting imminent failures?

The approach presented here builds upon previous papers [14, 15] which described a novel method for tracking hidden variable drifts in a hierarchical dynamical system.[1] This technique was developed in a dynamical systems framework for studying damage evolution [7]. The work focused on an electromechanical system, in which mechanical vibration measurements were used to track a drifting voltage of a supply battery. It was demonstrated both experimentally and analytically that the tracked quantity was in a one-to-one relationship with the actual battery voltage (measured independently). In fact, under circumstances to be expected in many cases, it was not only in one-to-one, but also in *linear* correspondence. In our previous work we have already alluded to the application of these methods to material damage problems; here we present the first results in this direction.

In this paper, we show that the presented techniques can be used to develop a *damage tracker*. This tracker provides practical information about what the *observable* facts of fatigue damage evolution are. Therefore, it can be used to verify applicability of available physics-based damage laws in MSHM. In addition, the obtained data can be used to guide the development of empirical damage evolution laws that would possess all appropriate length and time scales for applications in MSHM.

---

[1] For the merits of this technique as compared to other damage detection/diagnosis methods the interested reader is referred to [14, 15], where its is discussed in great detail.

3 Dynamical Systems Approach to Damage Evolution

In the dynamical systems approach [7], damage is viewed as a point evolving in an extended phase space of a hierarchical dynamical system. In this system, slow-time damage evolution causes parameter drifts in a subsystem describing dynamics of directly observable fast-time variables:

$$\dot{\mathbf{x}} = \mathbf{f}\left(\mathbf{x},\, \boldsymbol{\mu}(\boldsymbol{\phi}),\, t\right), \tag{1a}$$

$$\dot{\boldsymbol{\phi}} = \epsilon\, \mathbf{g}\left(\boldsymbol{\phi},\, \mathbf{x}\right), \tag{1b}$$

where: $\mathbf{x} \in \mathbb{R}^n$ is a directly observable, fast-time variable; $\boldsymbol{\phi} \in \mathbb{R}^m$ is a hidden fatigue damage, slow-time variable; $\boldsymbol{\mu} \in \mathbb{R}^s$ is a function of $\boldsymbol{\phi}$ representing the material parameters in Eq. (1a); a rate constant $0 < \epsilon \ll 1$ defines a time scale separation between fast and slow-time dynamics; and overdots denote differentiation with respect to time t. We assume that fast-time dynamics takes place in a region of the extended fast-time phase space that is a compact subset of $\mathbb{R}^n \times \mathbb{R}^1$.

This formulation is appropriate for systems with early or incipient fatigue damage accumulation [5]. This type of damage accumulation can be characterized by a time scale that is several orders of magnitude larger than a time scale associated with the dynamic response of the corresponding structure. In what follows, we summarize the main ideas behind our damage tracking strategy, noting any improvements to the already published procedure.

3.1 Damage Tracking Function

In an experimental context we usually do not have access to the analytical form of governing differential equations (1). However, we do have access to measurements from the fast-time system (1a). These measurements are usually sampled at uniform time intervals t_s, and the dynamics (i.e., the equivalent topological structure of the extended phase space) of Eq. (1a) can be reconstructed using a delay coordinate embedding [16, 17]. In this procedure, the measured scalar time series $\{x(r)\}_{r=1}^{M}$ is converted to a series of vectors $\mathbf{y}^T(r) = [\, x(r), x(r+\tau), \ldots, x(r+(d-1)\tau)\,] \in \mathbb{R}^d$, where τ (multiple of t_s) is a suitable delay time, and d is the appropriate embedding dimension. Embedding parameters, τ and d, are usually determined using the first minimum of the average mutual information [18] and method of false nearest neighbors [19], respectively.

The reconstructed state vectors are governed by an as yet unknown map of the form

$$\mathbf{y}(r+1) = \mathbf{P}\left(\mathbf{y}(r); \boldsymbol{\phi}\right). \tag{2}$$

The concept of *Phase space warping* refers to the small distortions in the fast-time system's vector field caused by slowly drifting parameters (i.e., damage evolution). Based on this concept, in [14, 15] the following *damage*

4

tracking function

$$\mathcal{E}_k(\boldsymbol{\phi}; \mathbf{y}(r)) = \mathbf{P}^k\left(\mathbf{y}(r); \boldsymbol{\phi}\right) - \mathbf{P}^k\left(\mathbf{y}(r); \boldsymbol{\phi}_0\right) \tag{3}$$

was proposed. In Eq. (3) $\mathbf{P}^k$ is the k-th iterate of the map defined by Eq. (2), $\boldsymbol{\phi}$ is current damage state, and $\boldsymbol{\phi}_0$ is the reference or healthy damage state.

In [14, 15], a suitably averaged $\mathcal{E}_k(\boldsymbol{\phi}; \mathbf{y}(r))$ was successfully used to track a scalar battery voltage variable. It was demonstrated that the relationship between the tracking function and the damage variable can be well approximated by an affine map, under certain linear observability conditions.

To actually calculate the tracking function $\mathcal{E}_k(\boldsymbol{\phi}; \mathbf{y}(r))$ for any given initial condition $\mathbf{y}(r)$, we need to know how the fast subsystem evolves over the time interval $k\,t_s$ for the current value of $\boldsymbol{\phi}$, as well as how this subsystem *would have* evolved for the reference value of $\boldsymbol{\phi}_0$. Since the system's fast-time behavior for the current value of $\boldsymbol{\phi}$ is directly measurable (i.e., we can reconstruct the fast-time trajectory using a sensor measurement from the fast subsystem),the strategy is to compare it to the predictions of a *reference model* describing the fast system's behavior for $\boldsymbol{\phi} = \boldsymbol{\phi}_0 + \mathcal{O}(\epsilon k t_s)$. Here, local linear models are used as the simplest form of a globally nonlinear reference model

$$\mathbf{y}(r + k) = \mathbf{A}_k \mathbf{y}(r) + \mathbf{a}_k, \tag{4}$$

where $\mathbf{A}_k$ is a $d \times d$ matrix and $\mathbf{a}_k$ is a $d \times 1$ vector. Eq. (4) approximates Eq. (2) for a particular point $\mathbf{y}(r)$ in the reference system's reconstructed phase space. Note that, in practical applications, other modeling solutions such as neural nets (e.g., [20]) or auto regressive moving averages (e.g., [21]) may be more appropriate. The parameters of local linear models are determined by calculating the best linear fit between N nearest neighbors of $\mathbf{y}(r)$ and their future states. Then the tracking function (Eq. 3) for the initial point $\mathbf{y}(r)$ can be written as

$$\begin{aligned}
\mathcal{E}_k(\boldsymbol{\phi}; \mathbf{y}(r)) &= \mathbf{y}(r + k) - \mathbf{A}_k \mathbf{y}(r) - \mathbf{a}_k + \mathbf{E}_k^M(\mathbf{y}(r)) \\
&= \mathbf{E}_k(\boldsymbol{\phi}; \mathbf{y}(r)) + \mathbf{E}_k^M(\mathbf{y}(r)),
\end{aligned} \tag{5}$$

where $\mathbf{E}_k^M(\mathbf{y}(r))$ represents the local linear model error, and

$$\mathbf{E}_k(\boldsymbol{\phi}; \mathbf{y}(r)) = \mathbf{y}(r + k) - \mathbf{A}_k \mathbf{y}(r) - \mathbf{a}_k \tag{6}$$

is the estimated tracking function that can be determined experimentally. The use of $\mathbf{E}_k(\boldsymbol{\phi}; \mathbf{y}(r))$ in place of $\mathcal{E}_k(\boldsymbol{\phi}; \mathbf{y}(r))$ is justified, if $\mathbf{E}_k^M$ is small compared to $\mathbf{E}_k$.

3.2   Damage Tracking Feature Vector

In previous work [14, 15, 22], a suitable norm of the averaged value of the estimated tracking function over one data record $\langle\|\mathbf{E}_k\|\rangle$ provided a good tracking metric for scalar damage variables. However, as discussed

in detail in [14], there generally will be superfluous fluctuations in the tracking results caused by: (a) the change in the population of points from data record to data record; and (b) the changes in the map of Eq. (2) and model error $\mathbf{E}_k^M$ from point to point.

The population changes are caused by the evolution of ϕ that acts as a bifurcation parameter for Eq. (1a). As parameters of Eq. (1a) traverse their range due to the accumulating damage, the system will undergo changes in its steady state behavior. These changes will be abrupt and can not be used to track ϕ, which evolves smoothly. This will also cause change in population of points from record to record. The old tracking metric could only deal with minor changes in population of points that extended the original coverage of the reference population.

Two main sources of superfluous fluctuations, which are not related to changes in ϕ are: (i) changes in the model fit error $\mathbf{E}_k^M$ from point to point, caused by a nonuniform coverage of reference phase space by the points on a reconstructed trajectory; and (ii) changes in the actual nonlinear mapping of Eq. (2), also from point to point. In the old metric the fluctuations due to the variability of modeling error where compensated for by a suitable weighted average of $\|\mathbf{E}_k\|$ over one data record, while the fluctuations caused by the change in the mapping of Eq. (2) were not alleviated.

Here, we compensate for all sources of of Eq. (2) fluctuation by using a new tracking feature vector. This new approach evaluates the average value of the estimated tracking function in N_s disjoint regions $\mathcal{B}_i$ $(i = 1, \ldots, N_s)$ of the reconstructed phase space

$$e_i^k = \|\mathcal{B}_i\|^{-1} \sum_{\mathbf{y}(r) \in \mathcal{B}_i} \|\mathbf{E}_k(\phi; \mathbf{y}(r))\| \; , \tag{7}$$

and combines them in one *damage tracking feature vector*:

$$\mathbf{S}_k = \left[e_1^k, e_2^k, \ldots, e_{N_s}^k \right]^T \; , \tag{8}$$

where each data record will have a total of N_s ($\mathbf{S}_k \in \mathbb{R}^{N_s}$) statistics.

The choice of parameter k depends on the data sampling rate and effect of noise on the sensitivity of the tracking function. The parameter k also affects the sectioning of the phase space into the disjoint regions, which should be done in such a way as to alleviate the sources of unrelated fluctuations with regards to the previous method. In particular, the estimated tracking function Eq. (6) for the points within the same region $\mathcal{B}_i$ should have approximately the same sensitivity with respect to damage variable. This would reduce fluctuations due to the change in the mapping Eq. (2), as well as the variation in the linear fit error $\mathbf{E}_k^M$ within one region. With the sectioning of phase space we are also more likely to have several regions that have approximately constant population of points from record to record. Thus, the effect of changes in steady state behavior on the feature vector statistics is also reduced.

It is conjectured based on previous work [14, 15, 22] that there is an affine projection $\mathcal{V}_\phi : \mathbb{R}^{N_s} \to \mathbb{R}^m$ that maps the proposed feature vector $\mathbf{S}_k$ onto the damage state $\phi \in \mathbb{R}^m$:

$$\phi = \mathbf{HS}_k + \mathbf{h}, \tag{9}$$

where ϕ is an estimate of actual damage state, $\mathbf{H}$ is an $m \times N_s$ matrix, and $\mathbf{h}$ is an $m \times 1$ vector.

3.3 Damage Identification

In many practical situations we do not have the direct measurement of damage state or means to estimate the affine projection parameters of Eq. (9). Therefore, the damage tracking feature vectors $\mathbf{S}_k$ have to be used directly to determine the observable facts about the hidden damage state. Here, we focus on a fatigue damage identification and consider two different approaches to this problem.

3.3.1 Smooth Orthogonal Decomposition

The SOD is a generalization of the optimal tracking method [25] that relies on the existence of underlying deterministic behavior of the damage accumulation process but does not require its model. This method is based on maximizing smoothness and overall variation in the feature vector, found by solving an eigenvalue problem. For completeness we give a brief description of the procedure in the following paragraphs.

The feature vector $\mathbf{S}_k$, Eq. (8), is estimated for N_r data records. These vectors are arranged in a $N_r \times N_s$ damage matrix, called $\mathbf{Y}$. Each column of this matrix is normalized by subtracting its mean and scaling it to unit norm. Next, we identify the *SOD-based tracking metric* by a linear projection of the matrix $\mathbf{Y}$

$$\boldsymbol{\varphi}_s := \mathbf{Yc}, \tag{10}$$

that varies smoothly. This can be accomplished by defining $(N_r - 1) \times N_r$ derivative matrix

$$\mathbf{D} := \begin{bmatrix} 1 & -1 & 0 & \dots & 0 \\ 0 & 1 & -1 & \dots & 0 \\ \vdots & \ddots & \ddots & \ddots & \vdots \\ 0 & \dots & 0 & 1 & -1 \end{bmatrix} \tag{11}$$

and minimizing the following ratio with respect to $\mathbf{c}$

$$g(\boldsymbol{\varphi}_{ot}) := \frac{\|\mathbf{D}\,\boldsymbol{\varphi}_s\|^2}{\|\boldsymbol{\varphi}_s\|^2}. \tag{12}$$

In minimizing g we maximize the smoothness and overall variation of $\boldsymbol{\varphi}_s$. The minimum of g is the smallest generalized eigenvalue λ of the following eigenvalue problem

$$[(\mathbf{DY})^T\mathbf{DY}]\mathbf{c} = \lambda[\mathbf{Y}^T\mathbf{Y}]\mathbf{c}. \tag{13}$$

The eigenvectors corresponding to the smallest eigenvalues give the optimal $\mathbf{c}$ and, hence, $\boldsymbol{\varphi}_s$.

3.3.2   Proper Orthogonal Decomposition

Proper Orthogonal Decomposition (POD), Singular Value Decomposition (SVD) or Karhunen-Loève Decomposition has been widely used to estimate the number of active states in nonlinear dynamical systems [23, 24] and, in general, for obtaining a low-dimensional approximations of high-dimensional processes. Proper orthogonal modes (POMs) have also been instrumental in studying linear and nonlinear mode interactions in systems [26]. Damage evolution even in linear materials (linear elastic fracture mechanics), is a highly nonlinear process. The dimensionality of this process cannot be investigated using linear statistics. However, the POD of the damage matrix $\mathbf{Y}$ should identify the active damage states (i.e., the POMs with highest energy content or modes corresponding to the largest singular values of $\mathbf{Y}$).

Here we give a brief description of the discrete version of the POD, which is the SVD. Using the SVD, the matrix $\mathbf{Y}$ can be written in the form

$$\mathbf{Y} = \mathbf{U}\boldsymbol{\Lambda}\mathbf{V}^T, \tag{14}$$

where $\mathbf{U}$ ($N_r \times N_r$) and $\mathbf{V}$ ($N_s \times N_s$) are unitary matrices, and $\boldsymbol{\Lambda}$ is a diagonal matrix of size $N_r \times N_s$ containing N_s singular values, which are arranged in decreasing order. The *POD-based tracking metric*, $\boldsymbol{\varphi}_p$, will be given by the columns of $\mathbf{U}$ or the POMs corresponding to the largest singular values of $\mathbf{Y}$.

The POD analysis will also test our hypothesis that the damage state of the considered experimental system is a scalar variable. In other words, our hypothesis will be confirmed if only one dominant POM is identified.

4   Damage Accumulation in a Magneto-Elastic Oscillator

The experimental system is a version of a well known, two-well magneto-elastic oscillator [27] obtained after modifying the apparatus used in [14]. The system is a clamped-free beam restricted to a single degree-of-freedom by stiffeners. Two permanent rare-earth magnets near the beam's free end providing a two-well potential (see Fig. 1). The beam displacement is measured by a strain gauge mounted close to the clamped end. A shallow notch is machined in the beam below the strain gauge and just above the stiffeners. The system is mounted on a shaker and is forced at 8 Hz. The forcing amplitude is set to obtain chaotic output.[2] The damage in the beam slowly accumulates for approximately 3.17 hours of operation, until the beam suffers complete fracture at the notch. Strain gauge output is sampled at 160 Hz sampling frequency ($t_s = 0.625 \times 10^{-2}$ sec), digitized (16 bit A/D), and stored on a computer.

---

[2]Note that the chaotic response is used in this case merely to simplify data acquisition: a more general method, such as stochastic interrogation [28] could be used for nonchaotic systems.

The experiment was stopped after every 10 minutes of data acquisition to take a digital image of the beam profile near the notch. During the image acquisition, the beam was always positioned in the same potential well, so that the surface of the notch was in tension. Subsequent to taking the image, forcing was restarted and data collection resumed after letting initial transients die out. Since the pulling force from the magnets was constant, the change in the beam configuration was due to the decrease in the beam stiffness at the notch caused by the fatigue damage accumulation as the experiment progressed. This change is determined by estimating the difference in the slope of the beam across the notch using the acquired digital images.[3] This change in the slope was used as an independent measurement of the beam damage shown in Fig. 2. In the inset we sample images taken during the experiment at (from left to right) 0, 3 and 3.2 hours.

Delay time and embedding dimension were estimated to be $6t_s$ and 5, respectively. The first 2^{14} data points were used for the reference data set, and $N = 16$ nearest neighbors were used for the local linear model parameter estimation. Throughout the experiment the system underwent many bifurcations that caused repeated periodic/chaotic transitions (see Fig. 3). Thus, loading on the crack was irregular and primarily chaotic.

In [27] the Duffing's two-well equation was shown to be a suitable model for this experimental system. Using this model we have investigated how the sensitivity of the tracking function Eq. (3) changes from point to point in its phase space. The model parameters were chosen so that it exhibited a chaotic response and the effect of the notch was modeled by a decreasing stiffness coefficient. It was found that for small k the sensitivity was mainly a function of initial position and initial velocity had a negligible effect on it. For larger k the largest sensitivities were observed to cluster close to the unstable manifold of the system. The presence of noise in the experimental data also limits the range of possible k values. Thus, even though the sensitivity was higher for large k values, the estimation of the tracking metric and sectioning of the phase space into the regions of approximately similar sensitivities is much easier for smaller k values. Therefore, for this study we set $k = 1$ and sectioned the phase space using equally spaced hyperplanes perpendicular to the position coordinate.

Upon completing the embedding and modeling process, we split the data into 456 non-overlapping records of $t_D = 4 \times 10^3 t_s$ size. The feature vector $\mathbf{S}_1$ was estimated by calculating the short-time prediction error $\mathbf{E}_1$ of the reference model for each record. The reconstructed phase space was partitioned into $N_s = 16$ disjoint regions. Partitioning was done using regular grid divisions along the third coordinate of $\mathbf{y}$. This formed the matrix $\mathbf{Y}$ of size 456×16. From each row of $\mathbf{Y}$ we subtracted the mean and scaled it to unit norm. Thus, each row of $\mathbf{Y}$ can be treated as a feature vector, and each column represents time history of one particular

---

[3]MATLAB image processing toolbox was used to determine the tangents to the sections of the beam edge before and after the notch.

feature. The results of these calculations are shown in Fig. 4.

5 Results and Discussion

In the current experiment, we have independent damage state measurement obtained from digital images (see Fig. 2). However, its resolution and sampling makes it inadequate for estimating the affine projection parameters of Eq. (9). In most practical situations, we do not have the direct measurement of damage state, and so are forced to infer information about a hidden damage state from available measured statistics. Thus, we turn to the analysis of the damage tracking feature vectors.

5.1 Fatigue Damage Identification

The components of the damage tracking feature vectors (see Fig. 4) clearly show power-law type monotonically increasing trends. However, some of the components seem to have better signal-to-noise ratios. For damage identification purposes, we have calculated generalized eigenvalues of Eq. (13) and singular values of matrix $\mathbf{Y}$. The results are shown in Fig. 5. From this picture, it is clear that the smallest eigenvalue is at least one order of magnitude smaller than the next smallest; similarly, the largest singular value is at least one order higher than the next largest. This clearly demonstrates that our feature vectors capture some scalar damage process occurring in the system.

The tracking metrics $\boldsymbol{\varphi}_p$ and $\boldsymbol{\varphi}_s$ corresponding to the largest singular value and smallest eigenvalue are plotted in Fig. 6, respectively. For comparison purposes we scale both metrics so that they vary from zero to one. The trend, which was apparent in the feature vector statistics Fig. 4, is clearly present in enhanced form in both tracking metrics. The two trackers are virtually indistinguishable. Thus, both damage identification methods yield practically equivalent damage state trackers and, in this particular experiment, the damage accumulation process seems to be described by a scalar state variable.

These results are in good agreement with the tracking obtained using the old scalar tracking metric [14], as shown by a dotted curve in Fig. 6 (this metric was also scaled for comparison purposes). These curve closely follows the identified scalar damage modes, only slightly deviating from them for a short period of time at 2.5 hour mark. The observed consistency in the tracking methods is attributed the absence of major deviations in data records from the population of points in the reference data set. The fact that in this particular experiment only scalar damage was identified, was also favorable for the old tracking metric. However, the new tracking metrics have the ability to also deal with higher dimensional damage variables.

5.2 Validation of Damage Identification

The static angular deflection across the notch calculated from digital images (see Fig. 2) is seen to increase in a way that is qualitatively similar to the tracking metrics. It was stated that generally we expect to find, linear one-to-one relationship between the tracking metrics and the independent measurement of damage. Fig. 7 presents a plot of the angular deflection data vs. the local average values of the tracking metrics. The average was taken around the time when the digital images were acquired. We clearly see the approximately linear, one-to-one relationship, consistent with the theory (refer to Eq. (9)).

The damage variable in Eq. (1b) is not tied to any particular physics of damage. For example, ϕ is not necessarily the length of the crack in this fracturing vibrating beam experiment. This simple experiment clearly demonstrates that even when the load on the crack tip is complex (i.e., a combination of periodic and chaotic forcing, see Fig. 3), and well before any visible cracks are present (i.e., during the initial damage accumulation and crack initiation stages), the *observable* damage evolution obeys a simple scalar power-law type behavior. Therefore, we speculate the existence of a suitable internal scalar variable, which need not be the crack length (in fact, during a small crack accumulation stage the crack growth rate is not a smooth function of crack length [29, 30]), that evolves monotonically and smoothly.

Currently there is no acceptable macroscopic damage evolution model for the initial damage accumulation process (when the damage occurs at the scale of microstructure). However, there are well developed models that govern the growth of macroscopic cracks. The most notable is the Paris equation which relates the *per cycle derivative* of a crack length, da/dN, to a range of stress intensity factor, $\Delta K = F\Delta s(\pi a)^{1/2}$ (where a is a crack length, N is a cycle count, Δs is a stress range, and value of F depends on the geometry and relative crack length), using a simple power law

$$da/dN = c(\Delta K)^m, \tag{15}$$

where c is a small constant. Since the forcing of our system was stationary and harmonic the *per cycle* derivative will be proportional to the *time* derivative of a crack length $\dot{a} = da/dt \sim da/dN$. Also, for a majority of metallic materials, the exponent m takes values from $m = 2$ to $m = 6$. For carbon steel, as is the case for our experiment, the magnitude of $m = 4$ is often recommended.

Now we hypothesize that for a macroscopic crack propagation stage our observed damage variable ϕ is related to the actual crack length. To verify this hypothesis, we rewrite the Paris equation replacing a with ϕ as

$$\dot{\phi} = c\left(F\Delta s(\pi\phi)^{1/2}\right)^4 = \epsilon\phi^2, \tag{16}$$

where $\epsilon = c\,\pi^2(F\Delta s)^4$ is some small constant. Integrating this equation in time gives

$$\phi^{-1} = -\epsilon t + \beta, \tag{17}$$

for some integration constant β. Thus, Eq. (17) gives a linear relationship between $1/\phi$ and time t. Our hypothesis is confirmed by plotting the reciprocal of our damage tracking metrics versus time. Fig. 8 depicts that the reciprocal of φ is a linear function of time for time interval from $t = 2.9$ to $t = 3.17$, just before the complete fracture.

For comparison purposes, a reciprocal of the old scalar metric is also plotted in Fig. 8. While it still shows a linear behavior right at the end of the experiment, the time interval of this agreement, $t \in (2.45, 3.17)$, is approximately twice shorter than for the new metrics, $t \in (1.9, 3.17)$. This is due to the deviations observed in Fig. 6. Therefore, the new identification schemes provide more consistent damage tracking data that is in good agreement with the simple power law model, Eq. (16), for macroscopic crack growth.

5.3   Failure Prediction

Based on the global damage tracking information, described above, it is possible to predict when this particular system will reach some predetermined failure state. For example, we can define a *failure surface* by $1/\varphi = 3$ (see the horizontal line in Fig. 8). Then, by fitting a straight line to the $1/\varphi$ versus time data and finding its intersection with the failure surface one can estimate the remaining time to failure.

Figure 9 shows the results of the remaining useful life estimation based on the *SOD-based tracking metric* data from Fig. 8. Here, a linear fit to the first 128 points from Fig. 8 was used for the first time to failure estimate. For the consequent estimates this 128-point window was moved repeatedly by one point. The solid straight line in Fig. 9 shows the true remaining time to failure drawn *a posteriori*. The black dots represent the estimates of remaining time to failure based on the 128-point linear fits. The shaded background shows the uncertainty in the estimate based on the linear fit error.

The graph in Fig. 9 is a result of very simple calculation and it gives accurate estimates of time to failure when about the third of useful life is still remaining. These results can be improved dramatically by employing a model-based recursive estimation technique discussed in [22], which is out of scope of this paper and will not be considered here.

6   Conclusions

In this paper we have presented a dynamical systems approach to material damage identification. This methodology does not depend on knowledge of particular damage physics of material fatigue. Instead, it provides experimental means to determine practically observable and observed facts of damage accumulation, thus making it possible to develop or experimentally verify appropriate damage evolution laws.

A detailed description of the damage identification algorithm was given. Experimental procedures for estimating the tracking functions in a reconstructed phase space, the calculation of the damage tracking feature vector, and the appropriate damage tracking metrics were given before describing an experimental application. The algorithm was applied to a magneto-elastic oscillator with fatigue damage accumulation in a beam. As the damage grew, the system underwent many bifurcations that caused repeated periodic/chaotic transitions. This resulted in a very complicated strain time series.

The recorded strain time series was used for damage tracking. Two different methods of damage identification smoothly and monotonically followed the accumulating damage and provided practically equivalent damage trackers. They both showed that only one scalar variable is sufficient to describe the fatigue damage accumulation in the beam. Despite the absence of an established physical damage state, the new metrics show that only one scalar variable is needed to describe the dynamics of both incipient and macroscopic damage accumulation. These results were also consistent with data obtained using the old scalar tracking metric, described in previous work [14]. The first visible crack in the beam occurred after 3 hour mark, but the tracking has shown monotonically increasing power-law type trends well ahead of that point, indicating the sensitivity of the tracking method.

Static change in the slope of the beam across the notch was used as an independent measurement of damage. It is seen to increase in a qualitatively similar way to the tracking metrics. In fact, this measurement was shown to be in approximately linear, one-to-one relationship with the identified tracking metrics. This confirmed our conjecture that the feature vector can be projected onto the actual damage state.

The tracking output was validated by verifying that the data corresponding to the macroscopic crack evolution fits well Paris fatigue crack growth model. Thus, we conclude that these methods can be used in direct experimental studies to provide much needed insight and feedback on the appropriate damage states and theories. Based on Fig. 8 we can assert that the optimal damage observer captures the correct damage evolution characteristics at least for the macroscopic crack propagation.

A very simple failure prediction scheme based on the damage tracking data and Paris model based power law was shown to accurately estimate the remaining time to failure well in advance of actual fracture. For the given experiment that ran about 3.17 hours, and advanced warning of 1 hour is shown to be possible even when using a simple empirical model of damage.

Acknowledgments

References

[1] J. L. Chaboche, Continuum damage mechanics: Part i – general concepts, Journal of Applied Mechanics 55 (1988) 59–64.

[2] J. L. Chaboche, Continuum damage mechanics: Part ii – damage growth, crack initiation, and crack growth, International Journal of Bifurcation and Chaos 55 (1988) 65–72.

[3] S. Suresh, Fatigue of Materials, Cambridge University Press, New York, 1991.

[4] J. Lemaitre, A Course on Damage Mechanics, Springer-Verlag, Berlin, 1996.

[5] V. V. Bolotin, Mechanics of Fracture, CRC Press, Boca Raton, 1998.

[6] W. Hwang, K. S. Han, Cumulative damage models and multi-stress fatigue life prediction, Journal of Composite Materials 20 (1986) 125–153.

[7] J. P. Cusumano, A. Chatterjee, Steps towards a qualitative dynamics of damage evolution, International Journal of Solids and Structure 37 (44) (2000) 6397–6417.

[8] Z. P. Bazant, Mechanics of distributed cracking, Applied Mechanics Review 39 (1986) 675–705.

[9] M. Kachanov, Elastic solids with many cracks: a simple method of analysis, International Journal of Solids and Structures 23 (1987) 23–43.

[10] T. L. Anderson, Fracture Mechanics: Fundamentals and Applications, CRC Press, Boca Raton, 1991.

[11] D. Broek, The Practical Use of Fracture Mechanics., Kluwer, Dordrecht, 1988.

[12] K. Hellan, Introduction to Fracture Mechanics, McGraw-Hill, New York, 1984.

[13] J. F. Knott, Fundamentals of Fracture Mechanics, Butterworth, London, 1979.

[14] D. Chelidze, J. P. Cusumano, A. Chatterjee, Dynamical systems approach to damage evolution tracking, part 1: Description and experimental application, Journal of Vibration and Acoustics 124 (2) (2002) 250–257.

[15] J. P. Cusumano, D. Chelidze, A. Chatterjee, Dynamical systems approach to damage evolution tracking, part 2: Model-based validation and physical interpretation, Journal of Vibration and Acoustics 124 (2) (2002) 258–264.

[16] F. Takens, Detecting strange attractor in turbulence, in: D. A. Rand, L. S. Young (Eds.), Dynamical Systems and Turbulence, Warwick, Springer Lecture Notes in Mathematics, Springer-Verlag, Berlin, 1981, pp. 336–381.

[17] T. Sauer, J. A. Yorke, M. Casdagli, Embedology, Journal of Statistical Physics 65 (3-4) (1991) 579–616.

[18] A. M. Fraser, H. L. Swinney, Independent coordinates for strange attractors from mutual information, Physical Review A 33 (2) (1986) 1134–1140.

[19] M. B. Kennel, R. Brown, H. D. I. Abarbanel, Determining embedding dimension for phase-space reconstruction using a geometric construction, Physical Review A 45 (6) (1992) 3403–3411.

[20] A. Alessandri, T. Parisini, Model-based fault diagnosis using nonlinear estimators: A neural approach, in: Proceedings of the American Control Conference, Vol. 2, 1997, pp. 903–907.

[21] W. Wang, A. K. Wong, Autoregressive model-based gear fault diagnosis, Journal of Vibration and Acoustics 124 (2) (2002) 172–179.

[22] D. Chelidze, J. P. Cusumano, A dynamical systems approach to failure prognosis, Journal of Vibration and Acoustics 126 (1) (2004) 1–7.

[23] G. Berkooz, P. Holmes, J. L. Lumley, The proper orthogonal decomposition in the analysis of turbulent flows, Annual Review of Fluid Mechanics 25 (1993) 539–575.

[24] J. P. Cusumano, M. T. Sharkady, B. Kimble, Experimental measurements of dimensionality and spatial coherence in the dynamics of a flexible-beam impact oscillator, Philosophical Transactions of the Royal Society 347 (1994) 421–438.

[25] A. Chatterjee, J. P. Cusumano, D. Chelidze, Optimal tracking of parameter drift in a chaotic system: Experiment and theory, Journal of Sound and Vibration. 250 (5) (2002) 877–901.

[26] B. F. Feeny, R. Kappagantu, On the physical interpretation of proper orthogonal modes in vibrations, Journal of Sound and Vibration 211 (4) (1998) 607–616.

[27] F. C. Moon, P. Holmes, A magnetoelectric strange attractor, Journal of Sound and Vibration 65 (2) (1979) 275–296.

[28] J. P. Cusumano, B. Kimble, A stochastic interrogation method for experimental measurements of global dynamics and basin evolution: Application to a two-well oscillator, Nonlinear Dynamics 8 (1995) 213–235.

[29] M. N. James, E. R. de los Rios, Variable amplitude loading of small fatigue cracks in 6261-t6 aluminum alloy, Fatigue and Fracture of Engineering Materials and Structures 19 (4) (1996) 413–426.

[30] K. Hussain, E. R. de los Rios, A. Navarro, A two-stage micromechanics model for short fatigue cracks, Fatigue and Fracture of Engineering Materials and Structures 44 (3) (1993) 425–436.
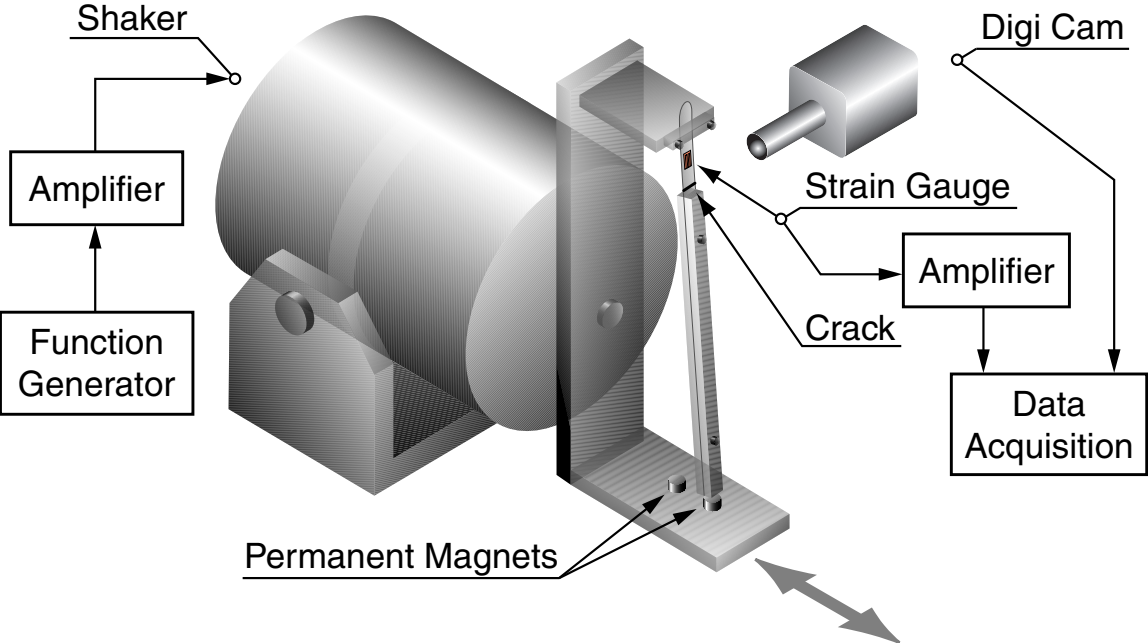
Figure Captions

Figure 1. Schematic diagram of the experimental apparatus of the two-well magneto-mechanical oscillator.
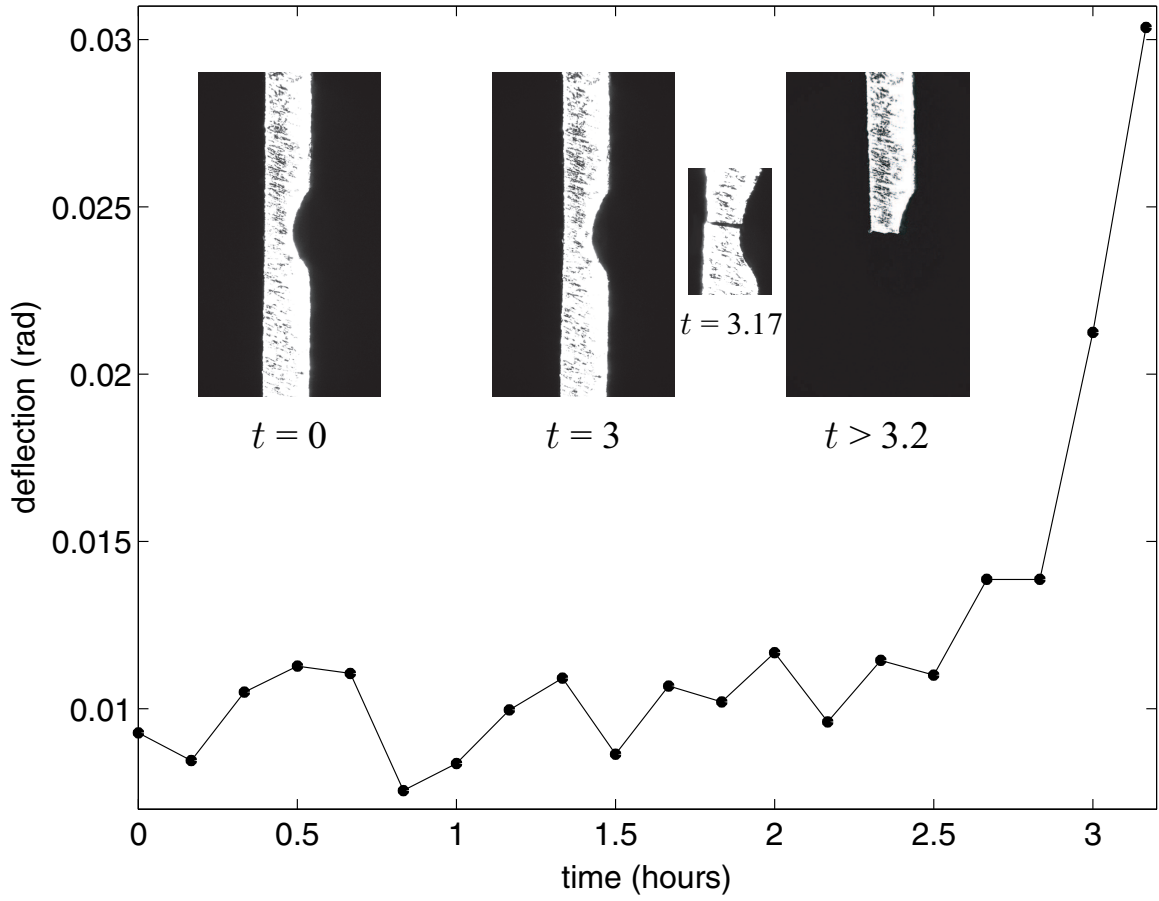
Figure 2. Plot of angular deflection across the notch during experiment, calculated from digital image. Inset shows photos on the notch taken at 0, 3 and 3.2 hours, also showing the first visible crack after 3 hours.

Figure 3. Passage through a periodic window occurring during the experimental run.

Figure 4. Columns of matrix $\mathbf{Y}$ composed of individual components of the feature vector $\mathbf{S}_1$.

Figure 5. Damage identification: singular values of matrix $\mathbf{Y}$, ●, and eigenvalues of Eq. (13), △.

Figure 6. Tracking results: SOD-based metric $\boldsymbol{\varphi}_s$, ——, POD-based metric $\boldsymbol{\varphi}_p$, $---$, and the old scalar metric $\langle\|\mathbf{E}_1\|\rangle$, $\cdots\cdots$.

Figure 7. Plot of the damage tracking metrics vs. angular deflection: $\langle\boldsymbol{\varphi}_s^{-1}\rangle$, ○, and $\langle\boldsymbol{\varphi}_p^{-1}\rangle$, △. The approximately linear, 1–1 relationship is consistent with the linear observability assumption (linear fits to: $\langle\boldsymbol{\varphi}_s\rangle$, ——, and $\langle\boldsymbol{\varphi}_p\rangle$, $---$).

Figure 8. Plot of the reciprocals of the tracking metrics vs. time: $\boldsymbol{\varphi}_s^{-1}$, ——, $\boldsymbol{\varphi}_p^{-1}$, $---$, corresponding linear fits, $-\cdot-$, and reciprocal of the old scalar tracking metric, $\cdots\cdots$. The data on the time interval from $t = 1.9$ to $t = 3.17$ is used for linear fits.

Figure 9. Remaining time to failure estimates based on a simple power law model, $\cdots\cdots$, actual time to failure known *a posteriori*, ——. Shaded background shows the uncertainty in the estimate.

Figures

Figure 1: Schematic diagram of the experimental apparatus of the two-well magneto-mechanical oscillator.

Figure 2: Plot of angular deflection across the notch during experiment, calculated from digital image. Inset shows photos on the notch taken at 0, 3 and 3.2 hours, also showing the first visible crack after 3 hours.
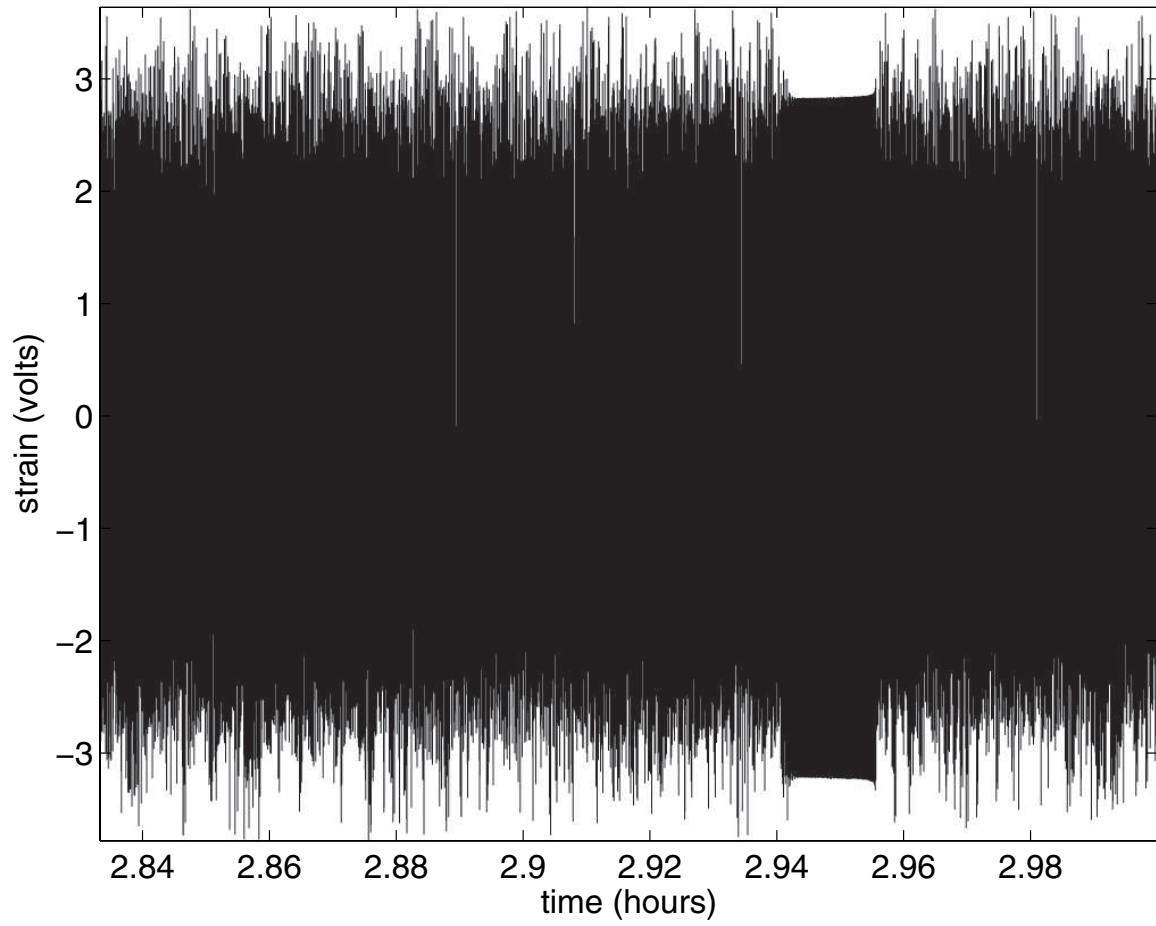
Figure 3: Passage through a periodic window occurring during the experimental run.
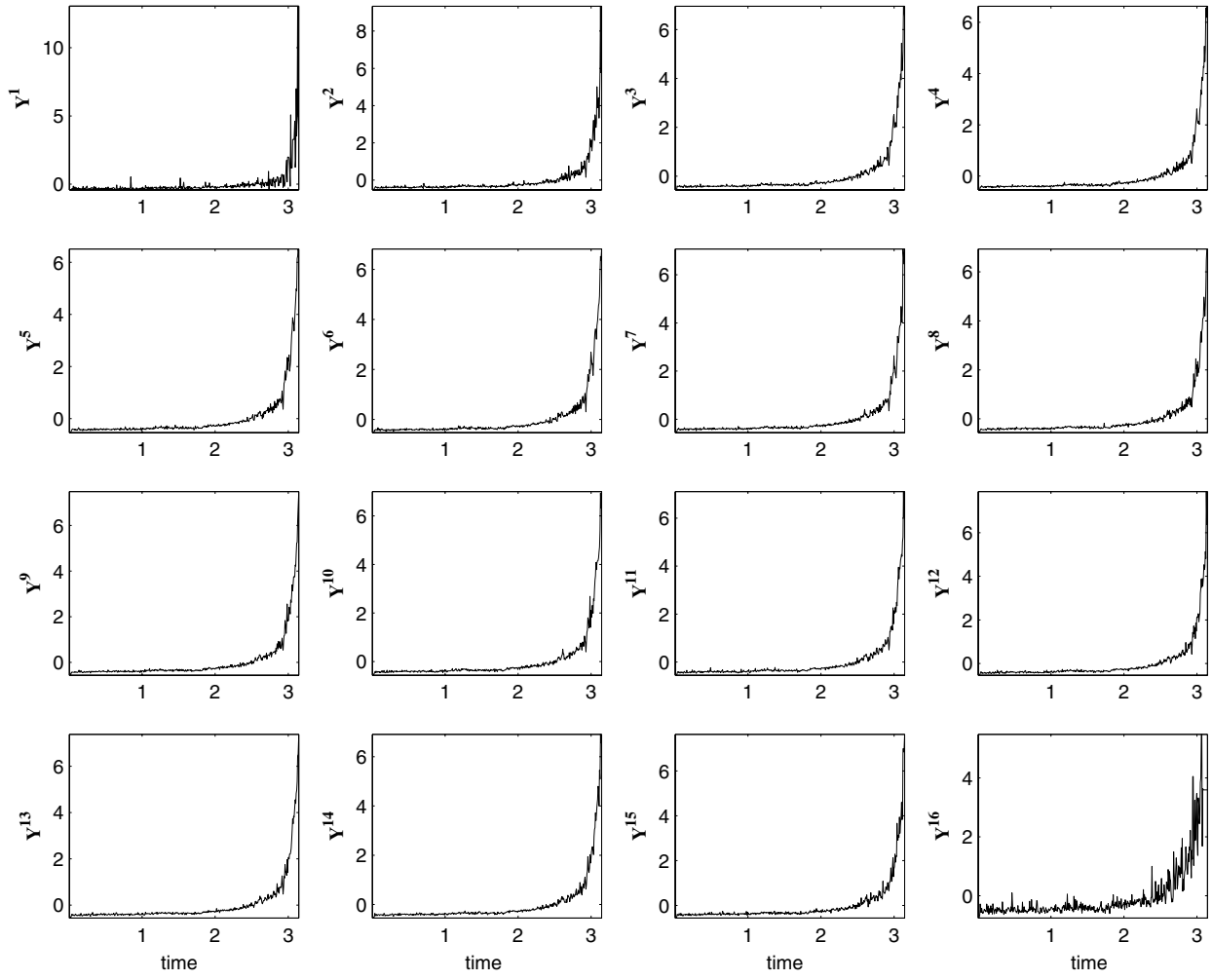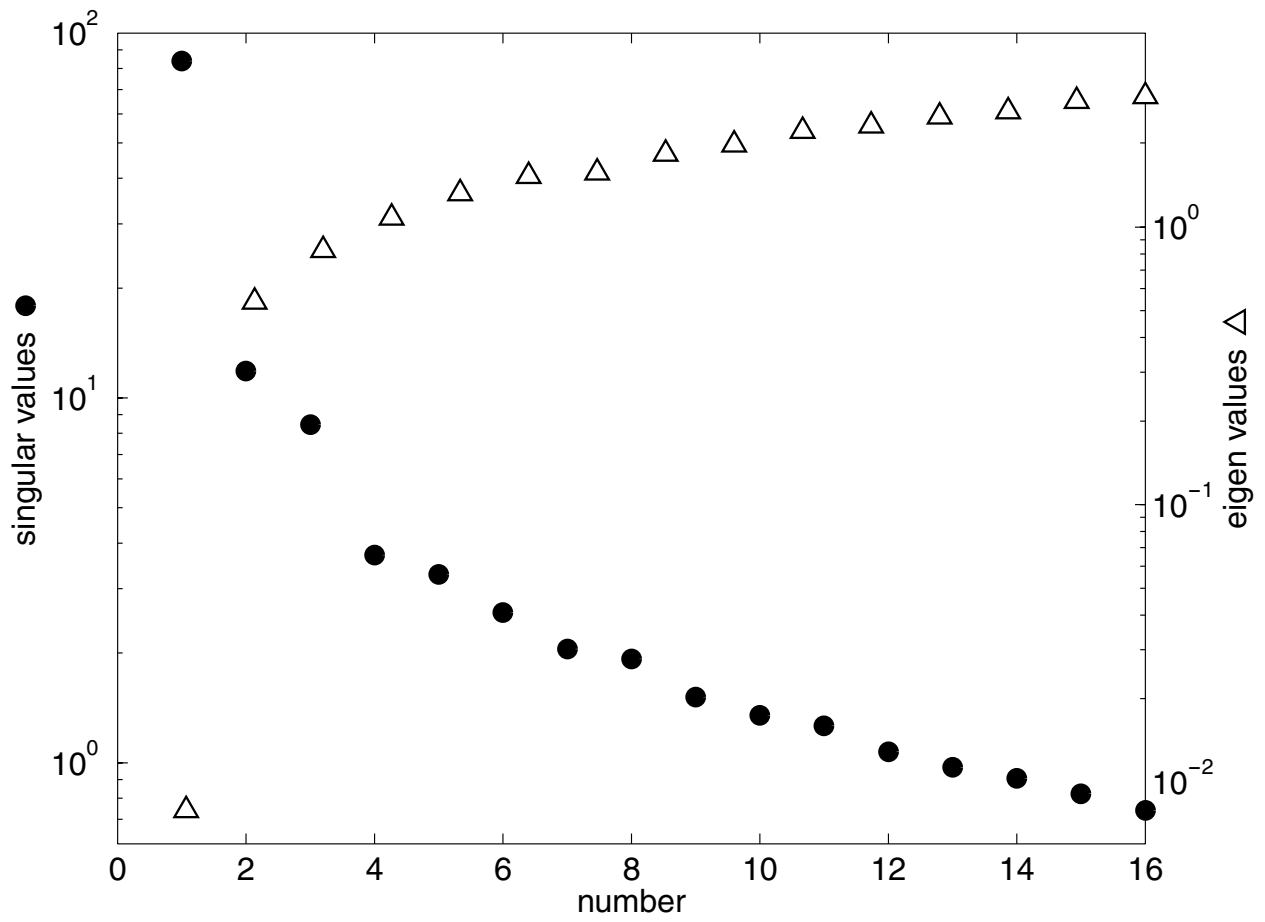
Figure 4: Columns of matrix $\mathbf{Y}$ composed of individual components of the feature vector $\mathbf{S}_1$.

Figure 5: Damage identification: singular values of matrix $\mathbf{Y}$, ●, and eigenvalues of Eq. (13), △.

Figure 6: Tracking results: SOD-based metric φ_s, ———, POD-based metric φ_p, $---$, and the old scalar metric $\langle \|\mathbf{E}_1\| \rangle$, $\cdots\cdots$.
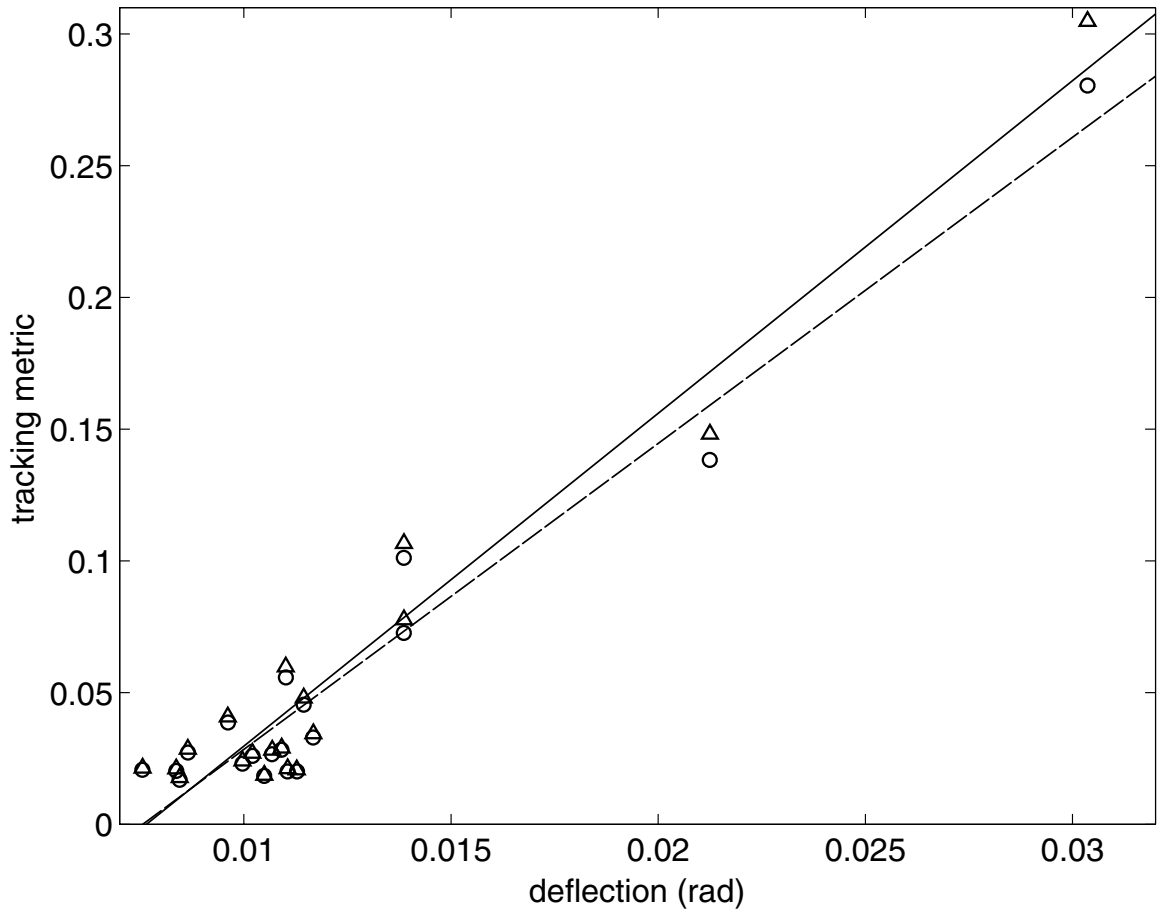
Figure 7: Plot of the damage tracking metrics vs. angular deflection: $\langle \boldsymbol{\varphi}_s^{-1} \rangle$, $\circ$, and $\langle \boldsymbol{\varphi}_p^{-1} \rangle$, $\triangle$. The approximately linear, 1–1 relationship is consistent with the linear observability assumption (linear fits to: $\langle \boldsymbol{\varphi}_s \rangle$, ——, and $\langle \boldsymbol{\varphi}_p \rangle$, ———).
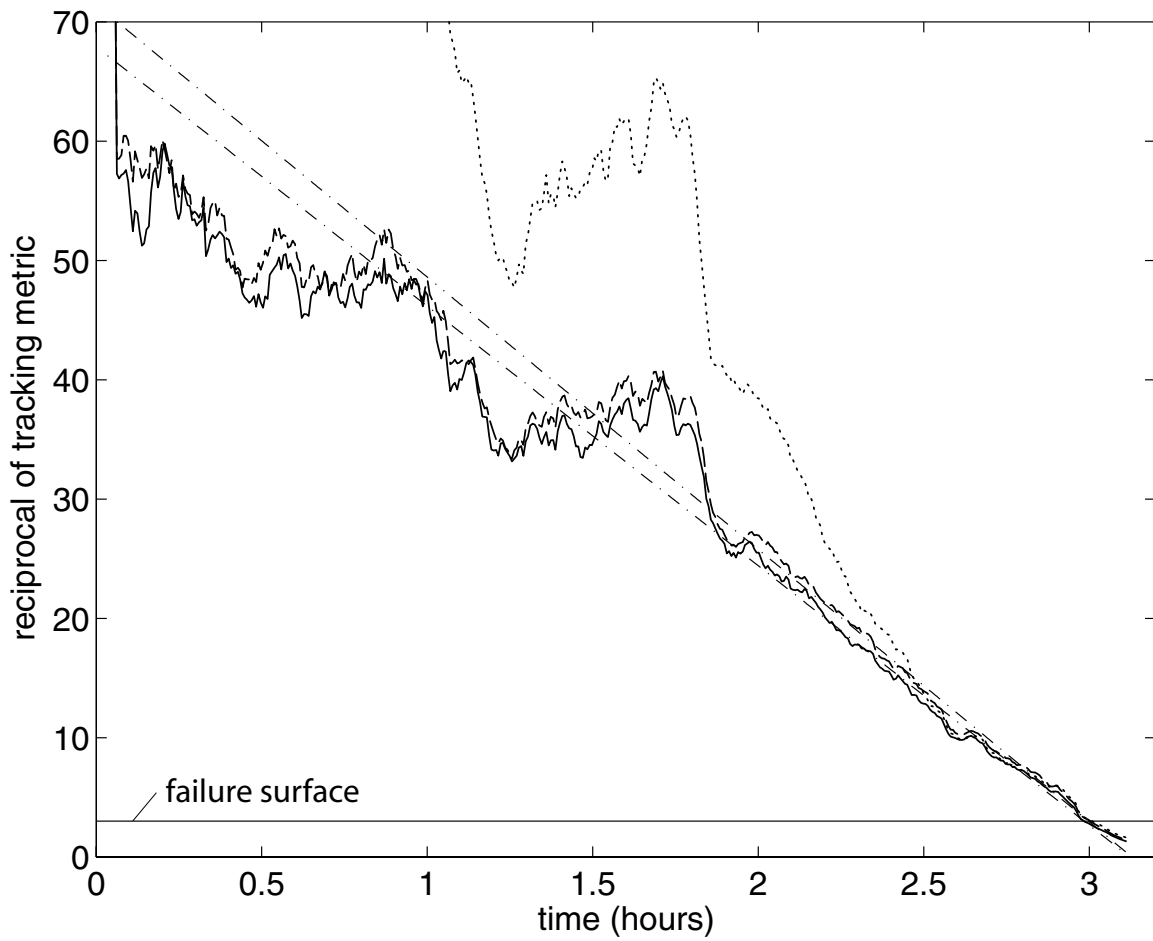
Figure 8: Plot of the reciprocals of the tracking metrics vs. time: φ_s^{-1}, ——, φ_p^{-1}, $---$, corresponding linear fits, $-\cdot-$, and reciprocal of the old scalar tracking metric, $\cdots\cdots$. The data on the time interval from $t = 1.9$ to $t = 3.17$ is used for linear fits.
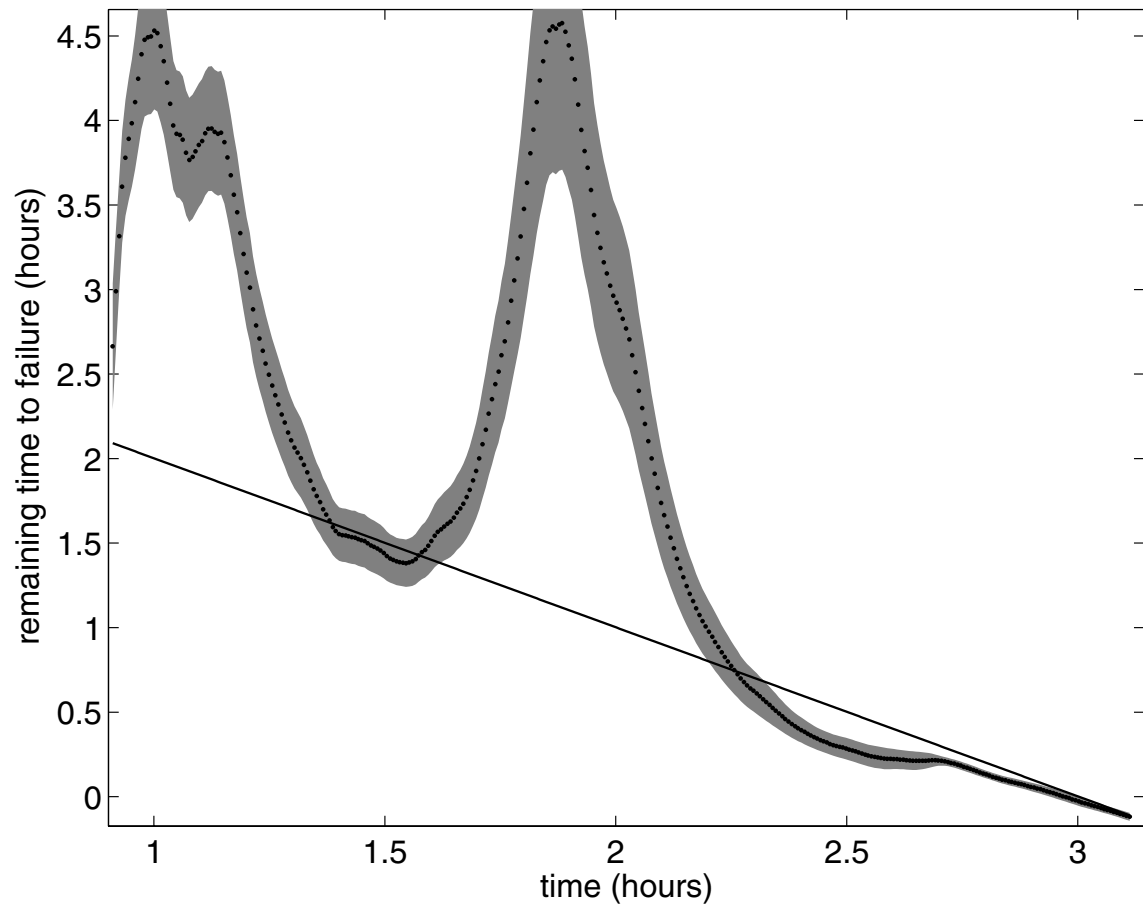
Figure 9: Remaining time to failure estimates based on a simple power law model, $\cdots\cdots$, actual time to failure known *a posteriori*, ———. Shaded background shows the uncertainty in the estimate.